water

MDPI

Article

Evaluation of the Application of the Moving Particle Semi-Implicit Method (MPS) to Numerical Simulations of Coupled Flow Between Low-Permeability Porous Media and Surface Water

Yoshihiko Hibi

Department of Environmental Science and Technology, Faculty of Science and Technology, Meijo University, Nagoya 468-8502, Japan; hibiy@meijo-u.ac.jp

Abstract: The moving particle semi-implicit method (MPS) has been employed to numerically simulate fluid flows. Further, some studies have used the MPS method to solve the Darcy–Brinkman equation, which also expresses fluid flow in porous media. However, these studies simulated flows only in porous media with high permeability, not in relatively low permeability. Thus, this study developed a numerical simulation method that employs Navier–Stokes equations to describe flow in surface water and the Richards equations, derived from the Darcy law and the law of conservation of mass, to describe water flow in porous media, and it uses the MPS method to discretize those equations. This numerical simulation method was then evaluated by comparing the numerical simulation results with previously obtained experimental results for fluid draining from the bottom of a column, which was first packed with silica sand saturated with water and then filled with water to 25 cm above the top surface of the sand, which had an intrinsic permeability of 1.737×10^{-11} m^2, a porosity of 0.402, van Genuchten parameters of 0.231 kPa^{-1} and 9.154, a residual gas saturation of 0.0, and a residual water saturation of 0.178. The numerical simulation was able to simulate the decrease in the level of the surface water above the silica sand in the column, similar to the column experimental results. However, the decrease in the saturated water in the silica sand obtained by the numerical simulation was almost consistent with the experimental results.

Keywords: moving particle semi-implicit method; Navier–Stokes equations; Richards equations; surface water–groundwater interaction; discontinuity problems

check for updates

Academic Editors: Kei Nakagawa, Jing Yang, Ming Dou and Channa Rajanayaka

Received: 27 January 2025
Revised: 6 March 2025
Accepted: 13 March 2025
Published: 17 March 2025

Citation: Hibi, Y. Evaluation of the Application of the Moving Particle Semi-Implicit Method (MPS) to Numerical Simulations of Coupled Flow Between Low-Permeability Porous Media and Surface Water. *Water* **2025**, *17*, 863. https://doi.org/10.3390/w17060863

Copyright: © 2025 by the author. Licensee MDPI, Basel, Switzerland. This article is an open access article distributed under the terms and conditions of the Creative Commons Attribution (CC BY) license (https://creativecommons.org/licenses/by/4.0/).

1. Introduction

Particle methods are often employed to investigate discontinuity problems such as a gas–water two-phase flow, crack progression, and embankment collapse due to overtopping flow during floods. Obviously, any interaction between the surface water and the groundwater must be considered in numerical simulations conducted to evaluate the safety of an embankment during flooding. For example, Maeda et al. [1] applied the smoothed-particle hydrodynamics method to characterize seepage failure in a medium around a sheet pile, and Harada et al. [2] simulated coastal morphodynamics using the moving particle semi-implicit method (MPS) coupled with the distinct element method. It is difficult to solve these discontinuity problems, however, by using lattice methods such as the finite element method, the finite difference method, or the finite volume method [3]. In an elastic deformation simulation based on a lattice analysis, large deformations occur at

nodal points, severely deforming each element and ultimately resulting in the breakdown of the deformation calculation. Furthermore, lattice methods cannot represent gas bubbles or water droplets that are smaller than the size of the lattice in a gas–water two-phase flow [4]. As mentioned above, the MPS method has mostly been applied to multiphase flows with an atmosphere–water interface and to large deformation and discontinuity problems. However, colloids and pollutants dissolved in groundwater, river water, and sea water are transported by water flows [5]. In addition, polluting substances in the groundwater flow into rivers and the sea, and vice versa. Pollution is also spread by the flow of the contaminated water in a reservoir at a water storage site when an embankment preventing the flow of pollutants collapses [6,7]. In such cases, the flow in surface waters, such as seawater and river waters, should be coupled with that in the groundwater [8]. Naturally, the surface water has a free water surface, which is similar to an interface between gas and water. In such cases, the mesh size used in the lattice method needs to be fine enough to reproduce accurately the interface at discontinuities, such as the boundaries between gas and water. In the case of large deformations, such as the collapse of an embankment, computations with the lattice method fail because the meshes where the deformation occurs overlap. By contrast, because MPS simulations have a resolution of one particle, they can reproduce water droplets and shear bands. Therefore, the MPS method is superior to the lattice method for reproducing the flow in a water–gas interface.

As far as this author has been able to determine, no study has conducted simulations for porous media with low permeability or for unsaturated porous media by using the MPS method, although some studies have conducted MPS simulations of the interaction between groundwater and surface water in a porous medium with high permeability [1]. However, there are many practical problems involving a low-permeability porous medium, or an unsaturated porous medium; therefore, it is important to be able to use the MPS method to simulate both low-permeability and unsaturated porous media. However, the Richards equation for groundwater has not been previously used in MPS simulations, except in one simulation study conducted by Hibi [9].

Colagrossi and Landrini [10] and Gotoh et al. [11] have pointed out that water pressure obtained by the classical MPS method of Koshizuka and Oka [12] spatially oscillates, and goes up and down in a more or less irregular manner furiously because the Poisson equation for water pressure includes a source term representing differences in the weight densities of the particles. To control these oscillations in water pressure, Khayyer and Gotoh [13] developed the higher order source term (HS); in numerical simulations using the MPS method with the HS, water pressures do not oscillate. In the fractional step method [14], the Navier–Stokes equation is decomposed into an equation containing a viscosity term and an intermediate velocity term and a second equation containing a water pressure gradient term and a gravity term. Both sides of the second equation are integrated with respect to space to obtain the water pressure while considering the conservation of mass. For this reason, this equation for obtaining the water pressure includes a source term that represents the divergence of the intermediate velocities. In their study, however, Koshizuka and Oka [12] changed this source term to one that represents differences in the weight densities of the particles considering the conservation of mass; these weight density differences are due to the water pressure oscillations. When the divergence of the intermediate velocities is employed as the source term in the Poisson equation for water pressure, the water pressure does not oscillate spatially, provided that the distances between particles are sufficient.

When the particles are closer than is appropriate, however, water pressure rises more and oscillates widely. If the particles are too close together, the water pressure calculation eventually fails and the water pressure cannot be obtained. This failure of the water pressure calculation does not occur with lattice methods, in which water pressure is obtained from

algebraic equations discretizing the Poisson equation. In the MPS method, the particles must be rearranged in order to maintain an appropriate distance between them. Thus, it is more difficult to obtain the water pressure by using the MPS method than by using a lattice method; in addition, the water pressure obtained by the MPS method may not be as accurate.

Computations by the MPS method require time to search for particles within an effective distance from a particle and to solve simultaneous equations for water pressure. With lattice methods, such as the finite element method (FEM) and the finite difference method (FDM), the computation can be divided into two parts: (1) setting up constitutional algebraic equations obtained from the geometric relations between nodal points and physical properties; and (2) solving the constitutional algebraic equations. The time required for setting up the constitutional algebraic equations is similar to the time required for solving simultaneous equations. However, the time spent searching for particles within the effective distance is longer than the time spent solving the simultaneous equations for water pressure. When the basic MPS method is used, the ratio of the time spent searching for particles within the effective distance to that spent solving the simultaneous equations for water pressure also increases with an increase in the number of particles for which all particles within the effective distance must be searched. Thus, the analysis region is divided into many zones, and the relationships among the zones is set up at the beginning of the simulation. Then, in practical cases, the zone in which a particle is located at the beginning of each time step is examined. Particles in the zone where the particle is located and in the neighboring zones are searched for, whether they are located within the effective distance or not. Thus, the number of particles to be searched is reduced to a limited number of particles, and the time required to search for the particles within the effective distance is likewise reduced. In addition, the particle search time and the time required for solving the simultaneous equations for water pressure can be reduced by using parallelization techniques, such as OpenMp and CUDA (Compute Unified Device Architecture), with graphics processing unit (GPU) accelerators [13,14].

When flood waters breach an embankment, interactions occur between the groundwater and the surface water at a soil surface with low permeability because most embankments consist of silt or a mixture of sand, loam, and clay. In such cases, the Darcy–Brinkman equation, as used by Hill and Straughan [15] and Onda et al. [16] in their numerical simulations of interactions between groundwater and surface water, does not need to be applied; rather, it is sufficient to apply the classical Darcy equation, because the water velocity in the soil is low and inertial forces do not need to be considered. As mentioned above, to date, no simulations with the MPS method for low permeability and/or unsaturated porous media have been conducted, yet it is necessary to be able to apply the MPS method to low-permeability and/or unsaturated porous media in order to numerically simulate all problems in which the surface water and groundwater are coupled with a discontinuous interface, such as the boundary between gas and water. Therefore, the aim of this study is to make it possible to apply the MPS method to a parabolic equation with a water pressure variable transformed from a Richards equation with two variables for volumetric moisture content and water pressure, and to simulate a low-permeability and/or unsaturated porous medium by using the MPS method.

2. Theory of Numerical Simulation

In this study, a Navier–Stokes equation [17] (Equation (1)) and a pressure-type Richards equation [18] (Equation (2)) were applied to describe the flows of surface water and groundwater, respectively:

$$\frac{D\mathbf{V}_w}{Dt} = -\frac{1}{\rho_w}\nabla P_w + \frac{\mu_w}{\rho_w}\nabla^2\mathbf{V}_w - \boldsymbol{g} \tag{1}$$

$$-nC_{wg}\frac{\partial P_w}{\partial t} = \nabla\cdot\left[K_w\frac{k}{\mu_w}(\nabla P_w + \boldsymbol{g}\cdot\nabla z)\right] \tag{2}$$

where $\mathbf{V}_w$ and P_w are the water velocity vector and water pressure, respectively; ρ_w and μ_w are the density of the water and the water viscosity, respectively; and g is gravitational acceleration. Thus, $\boldsymbol{g} = (0, 0, g)$. In Equation (2), C_{wg} is the specific water capacity in a water–gas two phase flow system and n is the porosity of a porous medium, k and K_w are the intrinsic permeability and the relative permeability of the medium, t is the elapsed time, and z is the coordinate in the z direction. The Navier–Stokes equation can be subdivided into two equations; then, by applying the differences method to the time term of the resulting equations, where the time interval is Δt, respectively, Equations (3) and (4) are obtained as follows:

$$\frac{\bar{\mathbf{V}}_w - \mathbf{V}_{w,t}}{\Delta t} = \frac{\mu_w}{\rho_w}\nabla^2\mathbf{V}_{w,t} \tag{3}$$

$$\frac{\mathbf{V}_{w,t+\Delta t} - \bar{\mathbf{V}}_w}{\Delta t} = -\frac{1}{\rho_w}\nabla P_w - \boldsymbol{g}\cdot\nabla z \tag{4}$$

Equation (5a,b) are used as the weight functions for the moving particle semi-implicit method (MPS), where the distance and the effective distance between particles i and j are $|\mathbf{r}_{ij}|$ and r_e, respectively. For accurately solving the water pressure and the water pressure gradient, a suitable value for the effective distance is 3.01 for a Laplacian equation or 2.01 for the water pressure gradient.

$$w_{ij}(|\mathbf{r}_{ij}|) = \frac{r_e}{|\mathbf{r}_{ij}|} - 1 \qquad (0 < |\mathbf{r}_{ij}| \le r_e) \tag{5a}$$

$$w_{ij}(|\mathbf{r}_{ij}|) = 0 \qquad (r_e < |\mathbf{r}_{ij}|) \tag{5b}$$

Furthermore, the weight density of a particle i is obtained as follows:

$$n_i = \sum_{i\neq j} w_{ij}(|\mathbf{r}_{ij}|) \tag{6}$$

The maximum weight density of a particle, which is defined as the reference weight density of particle n_0, is used to calculate an average of various values within the radius of effective distance.

Considering the mass conservation law and the incompressibility of water $\nabla\cdot\mathbf{V}_{w,t+\Delta t} = 0$, both sides of Equation (4) can be differentiated with respect to the spatial coordinate, and then the higher-order source term (HS) [13] and the MPS method for an irregular distribution of particles [19] can be applied as follows:

$$\begin{aligned}\frac{tr(\mathbf{T}\cdot\mathbf{B}^{-1})}{n_0}\left(\sum_{i\neq j}\frac{P_{w,t+\Delta t,j} - P_{w,t+\Delta t,i}}{|\mathbf{r}_{ij}|^2}w(|\mathbf{r}_{ij}|)\right) = \\ -\frac{g\rho_w tr(\mathbf{T}\cdot\mathbf{B}^{-1})}{n_0}\left(\sum_{i\neq j}\frac{z_j - z_i}{|\mathbf{r}_{ij}|^2}w(|\mathbf{r}_{ij}|)\right) + \frac{r_e}{n_0\Delta t}\sum_{i\neq j}\frac{\left(\bar{\mathbf{V}}_{w,j} - \bar{\mathbf{V}}_{w,i}\right)\cdot\mathbf{r}_{ij}}{|\mathbf{r}_{ij}|^3} + S_{ECS}\end{aligned} \tag{7}$$

where $P_{w,t+\Delta t,i}$ and $P_{w,t+\Delta t,j}$ are the water pressure of particles i and j at the elapsed time $t+\Delta t$, respectively, and z_i and z_j are the z coordinates of particles i and j, respectively. $\bar{\mathbf{V}}_{w,i}$ and $\bar{\mathbf{V}}_{w,j}$ are the intermediate velocities of particles i and j, which are the first term of the numerator on the left side of Equation (3). Further, the matrices $\mathbf{B}$ and $\mathbf{T}$ are defined by Equations (8) and (9), respectively.

$$\mathbf{B} = \frac{1}{n_0}\sum_{i\neq j}\frac{\mathbf{r}_{ij}\otimes\mathbf{r}_{ij}}{|\mathbf{r}_{ij}|^2}w(|\mathbf{r}_{ij}|) \tag{8}$$

$$\mathbf{T} = \left[\frac{1}{n_0}\sum_{i\neq j}\frac{\mathbf{r}_{ij}\otimes\mathbf{r}_{ij}}{|\mathbf{r}_{ij}|^2}w(|\mathbf{r}_{ij}|)\right]^{-1}\frac{\mathbf{r}_{ij}\otimes\mathbf{r}_{ij}}{|\mathbf{r}_{ij}|^2}w(|\mathbf{r}_{ij}|) \tag{9}$$

The above Equations (8) and (9) used to solve Equation (7) to guarantee the first-order accuracy of the Taylor series. The water pressure oscillates when the original MPS method with temporal and spatial variation of the difference in the weight density of the particles is used for the source term, because the variation in the weight density of the particles is amplified. As mentioned above, Equation (7) was derived by differentiating both sides of Equation (4), considering the mass conservation law and the incompressibility of water. Originally, the source term of Equation (7) is equal to the gradient of the intermediate velocity $\nabla\cdot\bar{\mathbf{V}}_{w}$. When this source term is used, the water pressure never oscillates. It is important to express the source term in terms of velocity. HS can be derived by differentiating the weight function and using the intermediate velocity. Thus, the water pressure distribution does not show spatial and temporal oscillation. In addition, S_{ECS} [19,20], defined in Equation (10), is added to Equation (7) to satisfy the solenoidal condition as follows:

$$S_{ECS} = \frac{r_e}{\Delta t n_0}\left|\frac{n_{i,t}-n_0}{n_0}\right|\sum_{i\neq j}\frac{(\mathbf{V}_{w,t,j}-\mathbf{V}_{w,t,i})\cdot\mathbf{r}_{ij,t}}{|\mathbf{r}_{ij,t}|^3} + \frac{r_e}{\Delta t n_0}\left|\sum_{i\neq j}\frac{(\mathbf{V}_{w,t,j}-\mathbf{V}_{w,t,i})\cdot\mathbf{r}_{ij,t}}{|\mathbf{r}_{ij,t}|^3}\right|\frac{n_{i,t}-n_0}{n_0} \tag{10}$$

where $n_{i,t}$ is the weight density of particle i at elapsed time t, and $\mathbf{V}_{w,t,i}$ and $\mathbf{V}_{w,t,j}$ are the water velocities of particles i and j at elapsed time t. The distance between particles i and j at t becomes $\mathbf{r}_{ij,t}$ here.

A higher order Laplacian (HL) model [21] can be applied to $\nabla^2\mathbf{V}_{w,t}$ in the viscosity term of Equation (3) to solve the Laplacian term like the viscosity term with precision, and then Equation (3) can be expressed for the intermediate velocities of particle i as follows:

$$\bar{\mathbf{V}}_{w,i} = \mathbf{V}_{w,t,i} + \Delta t\frac{\mu_w}{\rho_w}\frac{5-D_s}{n_0}\sum_{i\neq j}\frac{r_e(\mathbf{V}_{w,t,j}-\mathbf{V}_{w,t,i})}{|\mathbf{r}_{ij}|^3} \tag{11}$$

where D_s is the dimensional coefficient and $\bar{\mathbf{V}}_{w,i}$ are the intermediate velocities of particle i.

The governing formula of groundwater when the gas pressure is equal to an atmospheric pressure of zero can be expressed by Darcy's law and the mass conservation law as follows:

$$-nC_{gw}\frac{\partial P_w}{\partial t} = \nabla\cdot\nabla\left[\frac{K_{rw}}{\mu_w}k_s(\nabla P_w + \rho_w\mathbf{g}\cdot\nabla z)\right] \tag{12}$$

Here, the capillary pressure between gas and water P_{cgw} can be expressed as $P_{cgw} = -P_w$, and water saturation S_w in the porous medium can be calculated from this capillary pressure by using the van Genuchten model [22] as follows:

$$S_w = (1-S_{rw}-S_{rg})\left[1+(\alpha P_{cgw})^{\beta}\right]^{-1+\frac{1}{\beta}} + S_{rw} \tag{13}$$

where α and β are the van Genuchten parameters and S_{rw} and S_{rg} are the residual saturation of water and gas, respectively. In Equation (12), C_{gw} is the specific water capacity and can be calculated by Equation (14), which is obtained by differentiating Equation (13) with respect to the capillary pressure.

$$C_{gw} = (1 - S_{rw} - S_{rg})\alpha\beta\left(1 - \frac{1}{\beta}\right)\left[1 + (\alpha P_{cgw})^{\beta}\right]^{-2+\frac{1}{\beta}}(\alpha P_{cgw})^{\beta-1} \tag{14}$$

The relative permeability of water K_{rw} in the water–gas two-phase system has been expressed by Mualem [23] and Parker and Lenhard [24] as follows:

$$K_{rw} = S_w{}^{\frac{1}{2}}\left[1 - \left(1 - S_w{}^{\frac{1}{1-\frac{1}{\beta}}}\right)^{1-\frac{1}{\beta}}\right]^2 \tag{15}$$

Furthermore, n and k_s become the porosity and intrinsic permeability of the porous medium, respectively. The above Equation (12) can be transformed by using the MPS method with **B** and **T**, as defined in Equations (8) and (9), as follows:

$$\begin{aligned} &-nC_{gw,i}\tfrac{P_{w,t+\Delta t,i}}{\Delta t} - tr\left(\mathbf{T}\cdot\mathbf{B}^{-1}\right)\overline{K}_{rw,i}\tfrac{k_s}{\mu_w}\left(\frac{1}{n_0}\sum_{i\neq j}\frac{P_{w,t+\Delta t,j}-P_{w,t+\Delta t,i}}{|\mathbf{r}_{ij}|^2}w(|\mathbf{r}_{ij}|)\right) \\ &= -nC_{gw,i}\tfrac{P_{w,t,i}}{\Delta t} - tr\left(\mathbf{T}\cdot\mathbf{B}^{-1}\right)\overline{K}_{rw,i}\tfrac{k_s}{\mu_w}g\rho_w\left(\frac{1}{n_0}\sum_{i\neq j}\frac{z_j-z_i}{|\mathbf{r}_{ij}|^2}w(|\mathbf{r}_{ij}|)\right) \end{aligned} \tag{16}$$

where $P_{w,t,i}$ is the water pressure of particles i at the elapsed time t. $C_{gw,i}$ is the specific water capacity at the position of particle i and $\overline{K}_{rw,i}$ is the average relative permeability within the reference radius of particle i.

In this analytical method, the intermediate flow velocity in the surface water is first calculated using Equation (11). Then, the particles in the surface water are moved to the new position $\overline{\mathbf{r}}_i$ according to the particle position vector $\overline{\mathbf{r}}_i = \mathbf{r}_i - \overline{\mathbf{V}}_{w,i}\Delta t$. Next, for this distribution of particles, the water pressure is calculated using Equation (7) for surface water and Equation (16) for the porous medium, and the water pressure gradient of a particle i $\langle\nabla P_w\rangle_i$ is obtained by the MPS method using the gradient correction (GC) method [19] as follows (where Equation (8) is adopted for the irregular distribution of particles):

$$\langle\nabla P_w\rangle_i = \frac{1}{n_0}\mathbf{B}^{-1}\sum_{i\neq j}\frac{P_{w,t+\Delta t,j} - P_{w,t+\Delta t,i,}}{|\mathbf{r}_{ij}|^2}\mathbf{r}_{ij}w(|\mathbf{r}_{ij}|) + \frac{1}{n_0}\sum_{i\neq j}\mathbf{F}_{DS,ij}w(|\mathbf{r}_{ij}|) \tag{17}$$

Here, $\mathbf{F}_{DS,ij}$ becomes the volume forces between particles i and j, which are imposed on the particles to prevent them from approaching each other [25]. The position vector of a particle i $\mathbf{r}_{i,t+\Delta t}$ in the surface water at the elapsed time $t + \Delta t$ can be obtained as follows:

$$\mathbf{r}_i^* = \overline{\mathbf{r}}_i - \left(\Delta t\frac{\langle\nabla P_w\rangle_i}{\rho_w} + \Delta t\boldsymbol{g}\right)\Delta t \tag{18}$$

$\langle\nabla P_w\rangle_i$ is calculated using Equation (17) without the second term on the right side to determine the need of the rearrangement of particles, and $\mathbf{r}_i^*$ is obtained from Equation (18) by using this $\langle\nabla P_w\rangle_i$. The relative position vector $\mathbf{r}_{ij}^*$ is obtained as $\mathbf{r}_{ij}^* = \mathbf{r}_j^* - \mathbf{r}_i^*$ in this particle distribution $\mathbf{r}^*$ field. Then, $\mathbf{F}_{DS,ij}$ can be obtained from $\mathbf{r}_{ij}^*$ with Equation (19a,b), where d_{ij}, defined as $d_{ij} = \alpha_{DS}|\mathbf{r}_{0ij}|$, is obtained from the initial distance between particles

i and j $\left|\mathbf{r}_{0ij}\right|$ and the proximity coefficient between the particles α_{DS}, which is greater than 0.0 and less than 1.0.

$$\mathbf{F}_{DS,ij} = 0 \quad \left(\left|\mathbf{r}^*_{ij}\right| \geq d_{ij}\right) \tag{19a}$$

$$\mathbf{F}_{DS,ij} = \frac{\rho_w}{2\Delta t^2}\left(\sqrt{d_{ij}^2 - \left|\mathbf{r}^*_{ij,\perp}\right|^2} - \left|\mathbf{r}^*_{ij,\parallel}\right|\right)\mathbf{e}_{ij,\parallel} \quad \left(\left|\mathbf{r}^*_{ij}\right| < d_{ij}\right) \tag{19b}$$

The relative position vector $\bar{\mathbf{r}}_{ij}$, can be obtained as $\bar{\mathbf{r}}_{ij} = \bar{\mathbf{r}}_j - \bar{\mathbf{r}}_i$ in this particle $\bar{\mathbf{r}}$ distribution field, which is determined by the motion of particles from the intermediate velocities of Equation (11), where $\bar{\mathbf{r}}_i$ and $\bar{\mathbf{r}}_j$ are the position vectors of particles i and j, respectively, in this field. If $\mathbf{e}_{ij,\parallel}$ and $\mathbf{e}_{ij,\perp}$ are unit vectors parallel and perpendicular to $\bar{\mathbf{r}}_{ij}$, respectively, then $\mathbf{r}^*_{ij,\parallel}$ and $\mathbf{r}^*_{ij,\perp}$ in Equation (19b) can be derived as follows:

$$\mathbf{r}^*_{ij,\parallel} = \bar{\mathbf{r}}_{ij} - \left[\left(\bar{\mathbf{r}}_{ij} - \mathbf{r}^*_{ij}\right)\cdot\mathbf{e}_{ij,\parallel}\right]\mathbf{e}_{ij,\parallel} \tag{20a}$$

$$\mathbf{r}^*_{ij,\perp} = \sqrt{\left|\mathbf{r}_{ij} - \mathbf{r}^*_{ij}\right|^2 - \left[\left(\mathbf{r}_{ij} - \mathbf{r}^*_{ij}\right)\cdot\mathbf{e}_{ij,\parallel}\right]^2}\,\mathbf{e}_{ij,\perp} \tag{20b}$$

Then, considering $\mathbf{F}_{DS,ij}$ in Equation (19), $\langle\nabla P_w\rangle_i$ is calculated from Equation (17) and used to obtain the relative vectors $\mathbf{r}_{i,t+\Delta t}$ at $t+\Delta t$ with Equation (18). Furthermore, the water velocity $\mathbf{V}_{w,t+\Delta t,i}$ at the elapsed time $t+\Delta t$ in the surface water can be obtained using the following equation:

$$\mathbf{V}_{w,t+\Delta t,i} = \bar{\mathbf{V}}_{w,i} - \Delta t\frac{\langle\nabla P_w\rangle_i}{\rho_w} - \Delta t\boldsymbol{g} \tag{21}$$

The water velocity in the porous medium can be obtained from the following Darcy equation by using the $\langle\nabla P_w\rangle_i$ calculated by Equation (17).

$$\mathbf{V}_{w,t+\Delta t,i} = -\overline{K}_{rwi}\frac{k_s}{\mu_w}(\langle\nabla P_w\rangle_i + \rho_w\mathbf{g}) \tag{22}$$

Then, the particles in the porous medium move at the above water velocity in the porous medium $\mathbf{V}_{w,t+\Delta t,i}$ as follows:

$$\mathbf{r}_{i,t+\Delta t} = \mathbf{r}_{i,t} + \frac{\langle\nabla P_w\rangle_i}{\rho_w}\Delta t^2 - \boldsymbol{g}\Delta t^2 \text{ in the surface water} \tag{23a}$$

$$\mathbf{r}_{i,t+\Delta t} = \mathbf{r}_{i,t} + \mathbf{V}_{w,t+\Delta t,i}\Delta t \text{ in the porous medium} \tag{23b}$$

The space potential particle (SPP) method developed by Tsuruta et al. [26] (hereafter referred to as the standard SPP method) is used to search for particles at the free surface of the surface water. In the standard SPP method, a particle with n_i/n_0 less than 0.98 is determined to be located around the free water surface. This determined particle has a SPP on the gas side. For a particle i, this SPP is located at $\mathbf{r}_{i\mathrm{SPP}}$, and its position can be determined by Equation (24).

$$\mathbf{r}_{i\mathrm{SPP}} = \mathbf{r}_i - \frac{r_e}{n_0 - n_i + 1}\frac{\mathbf{r}_{ig}}{\left[\mathbf{r}_{ig}\right]} \tag{24}$$

where $\mathbf{r}_i$ is the position vector of particle i, and $\mathbf{r}_{ig}$ is the position vector of the center of gravity of particle density within an effective distance r_e. It can be obtained as follows:

$$\mathbf{r}_{ig} = \frac{1}{n_0} \sum_{i \neq j, i\mathrm{SPP}} \mathbf{r}_{ij} w\left(\left[\mathbf{r}_{ij}\right]\right) \tag{25}$$

Furthermore, the particle density of SPP $n_{i\mathrm{SPP}}$ is $n_{i\mathrm{SPP}} = n_0 - n_i$, and the water pressure at particle i corresponding to the SPP can be obtained by using the standard MPS method for a regular arrangement as follows:

$$\begin{aligned} -tr\left(\mathbf{T}\cdot\mathbf{B}^{-1}\right) P_{w,t+\Delta t,i} + \frac{tr\left(\mathbf{T}\cdot\mathbf{B}^{-1}\right)}{n_0} \sum_{i \neq j, ispp} w(\lceil \mathbf{r}_{ij} \rceil) P_{w,t+\Delta t,j} \\ = -\frac{g\rho_w tr\left(\mathbf{T}\cdot\mathbf{B}^{-1}\right)}{n_0} \sum_{i \neq j} w\left(\left|\mathbf{r}_{ij}\right|\right)\left(z_j - z_i\right) \\ + \frac{r_e}{n_0 \Delta t} \sum_{i \neq j} \frac{\left(\bar{\mathbf{V}}_{w.j} - \bar{\mathbf{V}}_{w,i}\right)\cdot \mathbf{r}_{ij}}{\left|\mathbf{r}_{ij}\right|^3} - \frac{tr\left(\mathbf{T}\cdot\mathbf{B}^{-1}\right)}{n_0}\left(n_0 - n_i\right) P_{w,\mathrm{SPP},i} \end{aligned} \tag{26}$$

Here, $P_{w,\mathrm{SPP},i}$ is the water pressure of an SPP particle for particle i. In addition, the SPP particles have the effect of filling small, meaningless spaces.

The analysis flowchart for the MPS method is shown in Figure 1. In the preparation for this numerical simulation, the relationships between each zone in which particles are located and the weight densities of the particles as well as the reference weight density of the particles must be obtained. Next, the intermediate velocities and the intermediate positions of the particles after moving at the intermediate velocities must be obtained. The weight densities of the particles are calculated again, and the zone in which the particles are located is searched. Then the porous medium parameters for unsaturated properties, such as water saturation, the specific water capacity, and the relative permeability to water, are calculated. Furthermore, after the calculation of S_{ECS}, the water pressures of the surface water and groundwater are calculated.

The positions of the particles after the rearrangement are decided by calculating the gradient of the water pressure without $\mathbf{F}_{DS,ij}$. If the relative distance between two particles in the particle rearrangement distribution field is less than 0.98 times the initial relative distance between the two particles in the initial particle distribution field, after calculating $\mathbf{r}^*_{ij,\parallel}$ and $\mathbf{r}^*_{ij,\perp}$ from $\mathbf{r}^*_i$ and $\bar{\mathbf{r}}_{ij}$, $\mathbf{F}_{DS,ij}$ is also calculated and used to calculate the water pressure gradient. If not, the water pressure gradient is calculated without $\mathbf{F}_{DS,ij}$, and the two particles are not rearranged in this case. Thus, the arrangement cost is only the decision of the arrangement positions, the calculation of r$\mathbf{r}^*_{ij,\parallel}$, $\mathbf{r}^*_{ij,\perp}$, $\mathbf{F}_{DS,ij}$, and the calculation of the water pressure gradient. As mentioned above, rearrangement is not necessarily applied to all particles, but it is applied to some particles.

The velocity of the particles in the porous medium is calculated by using the water pressure gradient and gravity and, additionally, by using the porous medium parameters. Furthermore, the new positions of the particles are determined by the water pressure gradient in the surface water and gravity and by the above-mentioned velocities in the porous medium. The above calculation and search are repeated until the elapsed time exceeds the maximum elapsed time of 4800 s.

Before the development of the MPS method, the smoothed-particle hydrodynamics method (SPH) was used for fluid flow. In the SPH method, interpolation functions (kernel functions), such as the B-spline function or the quantic spline function, are used and the water pressure is explicitly solved for the compressibility of the fluid. The kernel functions used in the SPH method are more complex than the interpolation function used in the MPS method (Equation (5a)). In addition, the water pressure is calculated by the semi-

implicit solution method in the MPS method, and by the explicit solution method in the SPH method. To control the water pressure oscillation, the compressibility of the fluid is considered in the SPH method, but a source term expressed as the fluid velocities is used in the MPS method. Thus, the total volume of the analysis is more easily compressed in the SPH method than in the MPS method.

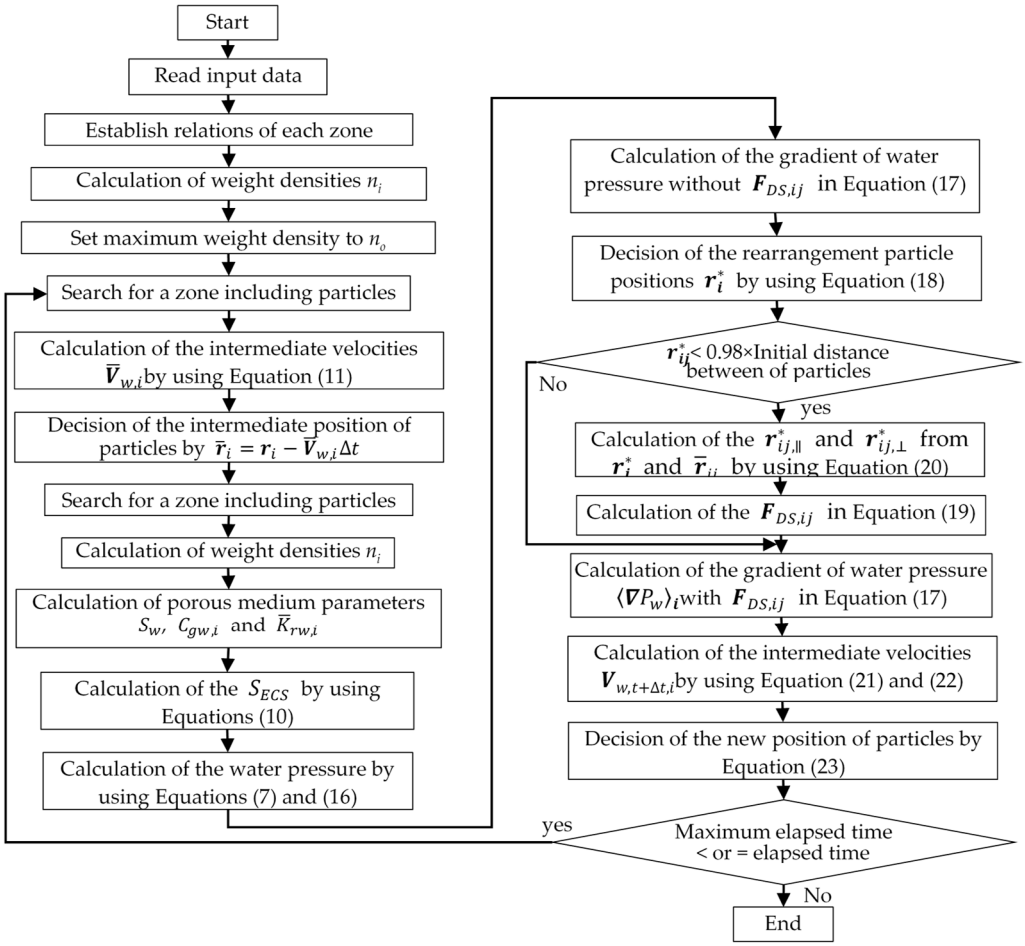


Figure 1. Analysis flowchart for the MPS method.

3. Results and Discussion

3.1. The Experiment with a Column Apparatus

The accuracy of this numerical simulation method using the Darcy equation and the MPS method was evaluated by using the results of a column experiment conducted by Hibi et al. [27]. The column apparatus consisted of an acrylic column with a length of 0.94 m, an inner diameter of 0.050 m, and a bottom plate with an outlet with an inner diameter of 0.034 m (Figure 2). A 75-μm-mesh stainless steel net was placed at the bottom of the column, 0.040 m above the bottom of the apparatus. In addition, to obtain the volumetric water content of the porous medium, soil moisture meters (Decagon Devices, EC-5, with an error of ± 0.02 m^3 m^{-3}) were placed at positions 24 cm and 39 cm from the bottom of the apparatus.

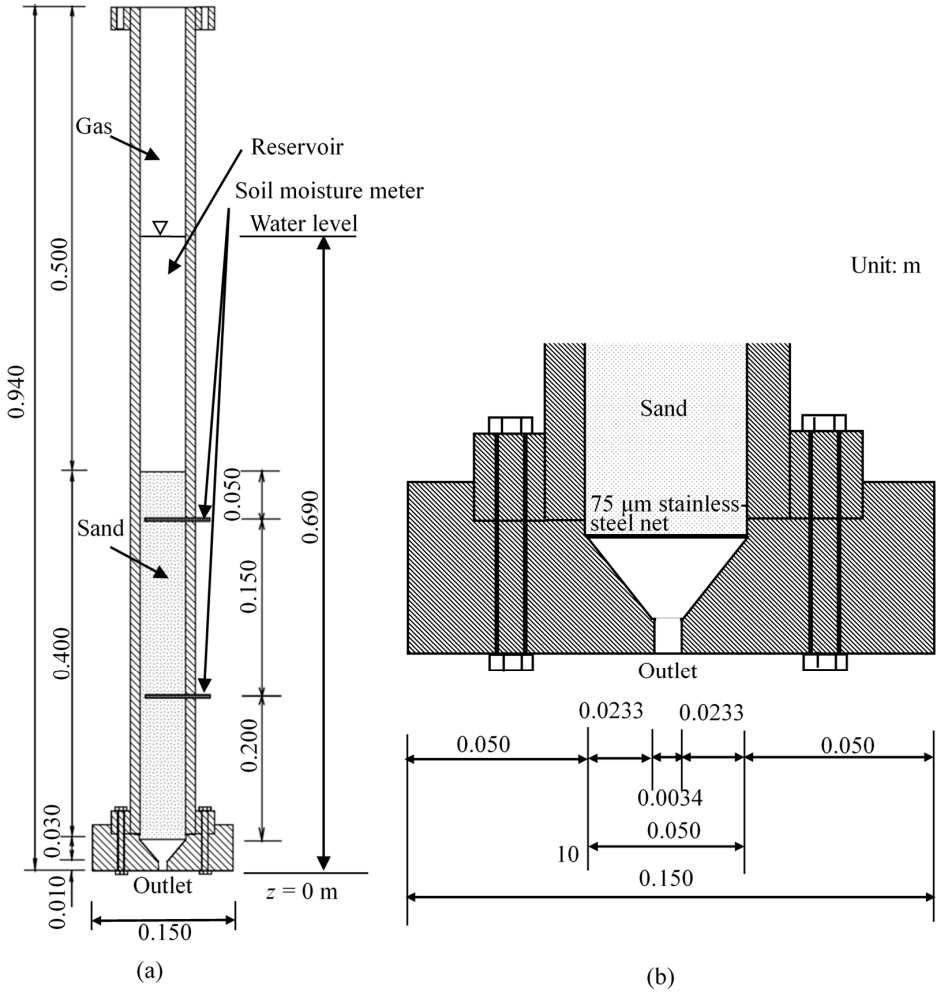


Figure 2. Schema of the column experiment apparatus. All values are in meters unless otherwise specified: (**a**) overall view; (**b**) enlarged view around the outlet.

Sand, sampled from Yamaguchi Prefecture, Japan, was passed through sieves to obtain a uniform grain size of 0.1–0.3 mm. Then the sand was used to fill the column from the bottom of the column (0.04 m from the bottom of the apparatus) to 0.4 m from the column bottom (0.44 m). The intrinsic permeability and porosity of the sand filling were 1.737×10^{-11} m^2 and 0.402, respectively. The van Genuchten parameters α and β were 0.231 kPa^{-1} and 9.154, respectively, and the residual gas saturation and the residual water saturation were 0.0 and 0.178, respectively.

The column apparatus was first filled with carbon dioxide, and then distilled water was poured into it to a height of 0.69 m from the bottom of the apparatus. Then, the water pressure at the bottom of the apparatus was lowered to −1.816 kPa, and the free water level was moved down by discharging water from the bottom for 80 min. After that, the drawdown of the free water surface in the reservoir above the sand was observed, and the volumetric water content of the sand was measured by the soil moisture meters described above. The density and viscosity of the water during the experiment were 0.999 g cm^{-3} and 9.32×10^{-7} kPa^{-1}, respectively. The above parameters were obtained from the parameters set by Hibi et al. [27].

3.2. Analytical Domains, Initial Distributions of Particles, and Boundary Conditions

In this study, two cases were numerically simulated: in the first case, only the column without the bottom plate was considered (Figure 3a); in the second case, the entire column apparatus was considered (Figure 3b). When the bottom plate is removed (as in Figure 3a),

the water flow is one-dimensional downward. By contrast, when the entire column apparatus is used in the simulation, the water in the water pool below the column flows either three- or two-dimensionally, and the water pressure is negative because of the extraction of water from the bottom of the water pool. However, the water in the column above the water pool flows one-dimensionally when the entire column is used, just as it flows when only the column is used in the simulation.

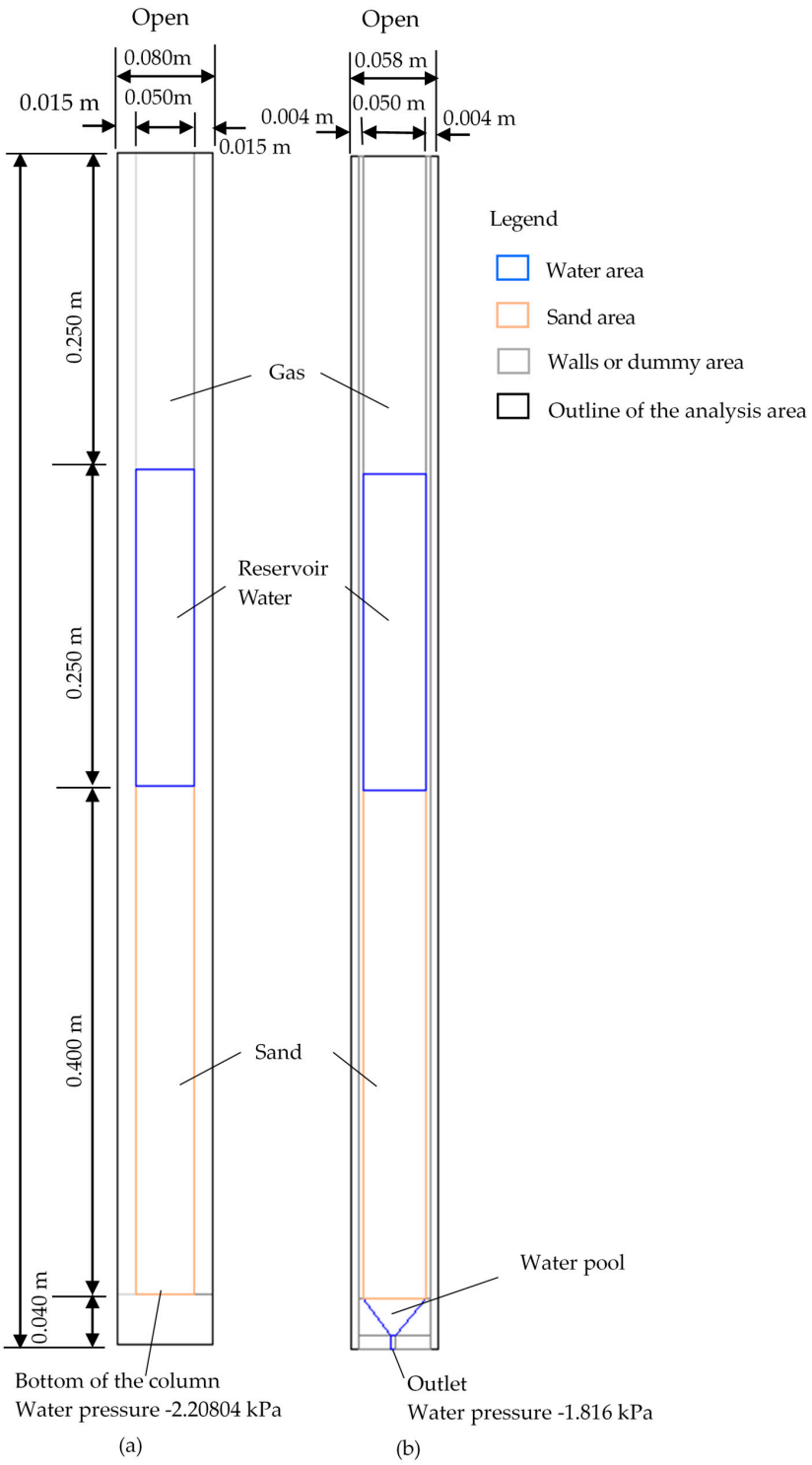


Figure 3. Diagram of the analytical domains and the boundary conditions for the two numerical simulations: (**a**) the simulation for only the column (without the bottom plate and outlet); (**b**) the simulation for the entire column apparatus (with the bottom plate and outlet).

In the column-only simulation, the reservoir and sand regions had heights of 0.25 m and 0.40 m, respectively. The area below the sand region was empty. Particles entering this empty region from the sand region became water particles in the atmosphere and moved at the outflow velocity from the sand. Particles exiting from the region below the analytical domain were removed from the numerical simulations. The reservoir and the sand were both 0.05 m wide, as in the column experiment, and the area below the sand was 0.080 m wide. Wall zones set on both sides of the reservoir and the sand were 0.005 m wide. Furthermore, dummy zones with a width of 0.010 m were set on the outside of the wall zones. In this case, particles were regularly distributed at a spacing of 0.005 m in the reservoir and sand regions, as well as in the wall and dummy regions. Thus, a one-particle-wide wall zone was located on each side of the reservoir and sand regions, from the top of the analytical domain to the bottom of the sand. The water pressure, but not the water velocity, was calculated at the wall particles. The dummy particles were used only for calculating the particle density of the water particles, porous medium particles, and wall particles, and they did not affect the accuracy of the water pressure and water velocity. However, the dummy particles influence the search by the standard SPP method for the particles around the free water surface. As mentioned above, in this paper, the water pressure is also calculated at the wall particles. Moreover, the wall particles and the dummy particles never move. The water particles and the porous medium particles can move parallel to the wall, and the wall particles prevent the water particles and the porous particles from breaking through the wall. Therefore, the wall particles affect the accuracy of the water pressure and the water velocity. Both the water pressure and the water velocity were calculated at the water particles and the porous medium particles. The total number of particles was 2672, and a water pressure of −2.20804 kPa, which was the hydrostatic pressure obtained for a water pressure of −1.816 kPa at the outlet at the bottom of the water pool, was imposed at the lowest porous medium particles in the sand region and at the lowest wall particles. As mentioned above, dummy particles and wall particles could not move, but water particles and porous medium particles could move at a velocity equal to the water velocity (Figures 3a and 4).

In the entire column apparatus simulation, the region of the water pool under the column was added to the analytical domain. This water pool region had a shape consisting of a trapezoid 0.050 m wide at the top and 0.004 m wide at the bottom above a rectangle 0.004 mm wide and 0.010 mm long that modeled the outlet installed at the bottom of the column experiment apparatus. In this simulation, 43,269 particles were placed at a spacing of 0.001 m (Figure 5). In the outlet at the bottom of the analytical domain, water particles were placed in horizontal rows of three particles, and wall particles were placed in rows of two particles on either side of the region of the water particles (Figure 5d). Water particles were also placed in the water pool, which was flanked on both sides by wall particles in rows of two particles. Similarly, wall particles were placed in rows of two particles on both sides of the reservoir and sand regions, and also on both sides of the column without water particles or porous medium particles. Dummy particles were distributed on the outside of the outermost wall particles. The spacing of the particles in the entire column apparatus simulation was narrower than that in the column-only simulation to allow particles to exit the analytical domain smoothly. Because of the 0.001 m particle spacing, the horizontal width of the outlet used in the simulation with the entire column apparatus (0.004 m) was slightly wider than its width in the experimental apparatus (0.034 m). A water pressure of −1.816 kPa was imposed on the lowest water particles and wall particles in the analytical domain in the entire column apparatus simulation.

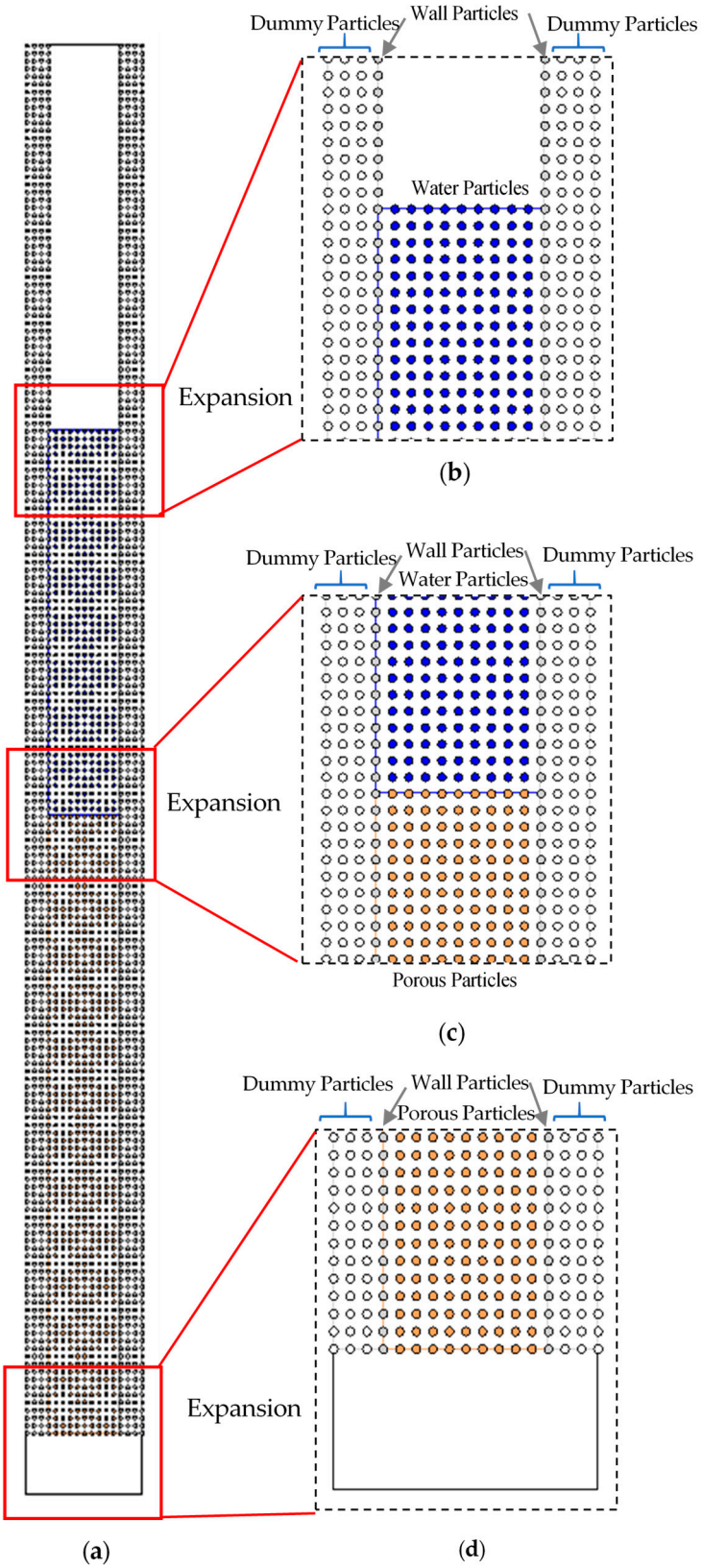


Figure 4. The analytical domain and initial distribution of particles in the column-only simulation: (**a**) overview; (**b**) surface water; (**c**) boundary between surface water and sand; (**d**) bottom of the column. The blue circles are surface water, the orange circles are a porous medium, the gray circles are walls and the white circles are dummies.

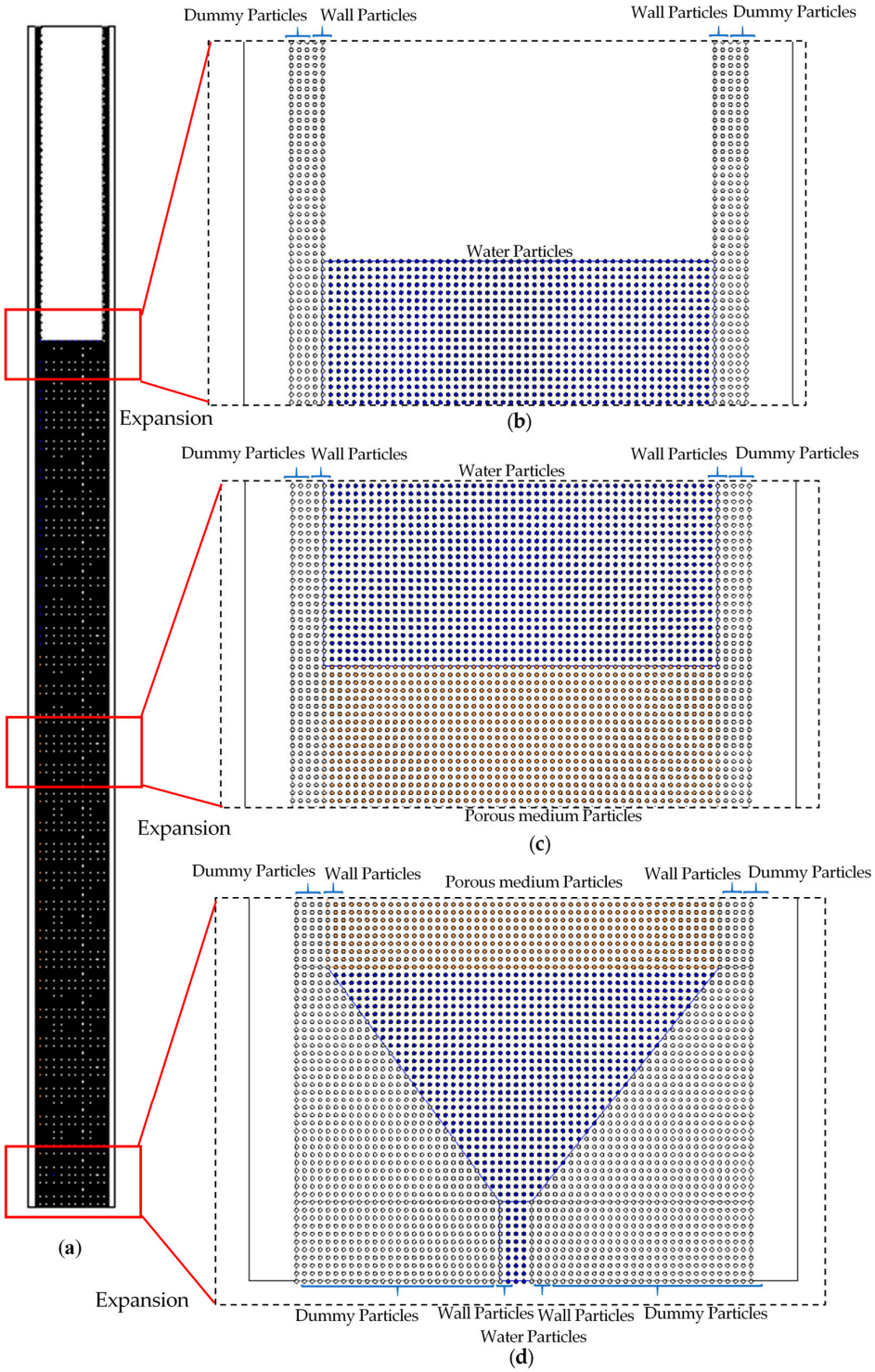


Figure 5. The analytical domain and initial particles distribution for the entire column apparatus simulation: (**a**) overview; (**b**) surface water; (**c**) boundary between surface water and sand; (**d**) bottom of the column. The blue circles are surface water, the orange circles are a porous medium, the gray circles are walls and the white circles are dummies.

3.3. Results of the Entire Column Apparatus Numerical Simulation with the Space Potential Particle Method

In the standard SPP method, $P_{w,\mathrm{iSPP}}$ can be deleted from the right side of Equation (26) because the water pressure of the SPPs is imposed as zero because the atmospheric pressure is equal to zero. In this study, the standard SPP method was used in the entire column apparatus simulation at first. As a result, most of the water particles in the water pool

had exited the analytical domain by the elapsed time of 1.5 s (Figure 6), when only a few particles remained in the water pool. These results represent the physical phenomenon in which the water is discharged from the bottom of the water pool whose upper surface, except for the columnar part, is exposed to the atmosphere. Figure 6 shows that the water pressure can be calculated correctly by the MPS method even when the particles in the water pool are sparse, in other words, even when the particle weight density is extremely low. Although the water pressure was imposed as zero for the SPPs, at the corresponding particles, it was not zero and could be obtained by solving Equation (26). In this study, the water pressure in the water pool should be negative because a water pressure of −1.816 kPa was imposed at the outlet of the entire column apparatus. If gas zones occur in the water pool, some SPPs will be set in those gas zones and, in the standard SPP method, the water pressure at these particles should be set to zero. Thus, in the water pool, the water pressure at the outlet would be lower than that of the SPPs, which would cause the water pressure gradient to be such that it increased toward the outside of the analytical domain. Therefore, it was necessary to set the water pressure of the SPPs at lower than −2.207 kPa, which is the static water pressure at the top of the water pool when the water pressure at the outlet is −1.816 kPa. Thus, in this study, different from the standard SPP method, the water pressure of the SPPs was imposed as −3.00 kPa in the water pool below the sand and as 0.00 kPa in the reservoir above the sand. Similarly, the water pressure of the particles corresponding to the SPPs was imposed as −3.00 kPa in the water pool and 0.00 kPa in the reservoir. As a result, only an appropriate number of particles is discharged from the water pool and the water pool remains filled with particles (Figure 7). In reality, the water pressure in the water pool is physically connected to that in the column above the water pool. It was found that the MPS method could simulate the real phenomenon of a negative water pressure by improving the SPP method as described above.

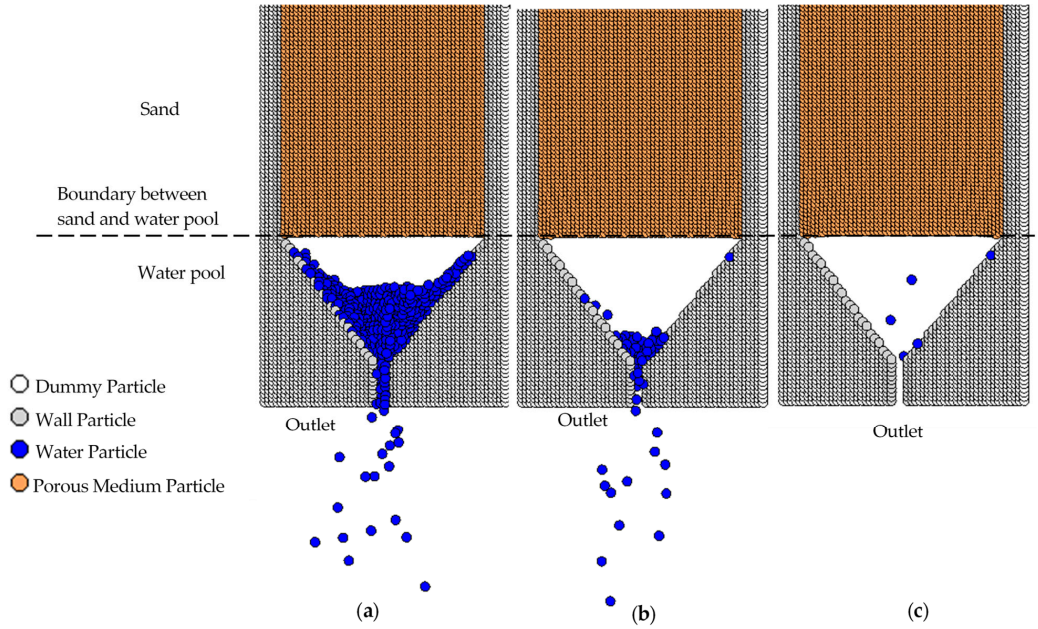


Figure 6. Particle distribution near the outlet of the column apparatus obtained by the entire column apparatus numerical simulation using the standard SPP method. Elapsed time at (**a**) 0.5 s, (**b**) 1.0 s, and (**c**) 1.5 s.

In addition to the entire column apparatus simulation, a column-only numerical simulation was conducted so that the effect of the water pool could be evaluated (Figure 8). The particle distribution shown in Figure 8 has some slightly dense and sparse areas, which means that the particle weight density distribution exhibits weight density differences. The

water pressure distributions shown in Figure 8a,b do not indicate oscillation of the water pressure independent of the difference in the weight density. Therefore, as mentioned above, because it was found that the particles were not approaching each other, the particles could be successfully rearranged by the GC method with $\mathbf{F}_{DS}$. As a result, the water pressure was never raised extremely anywhere.

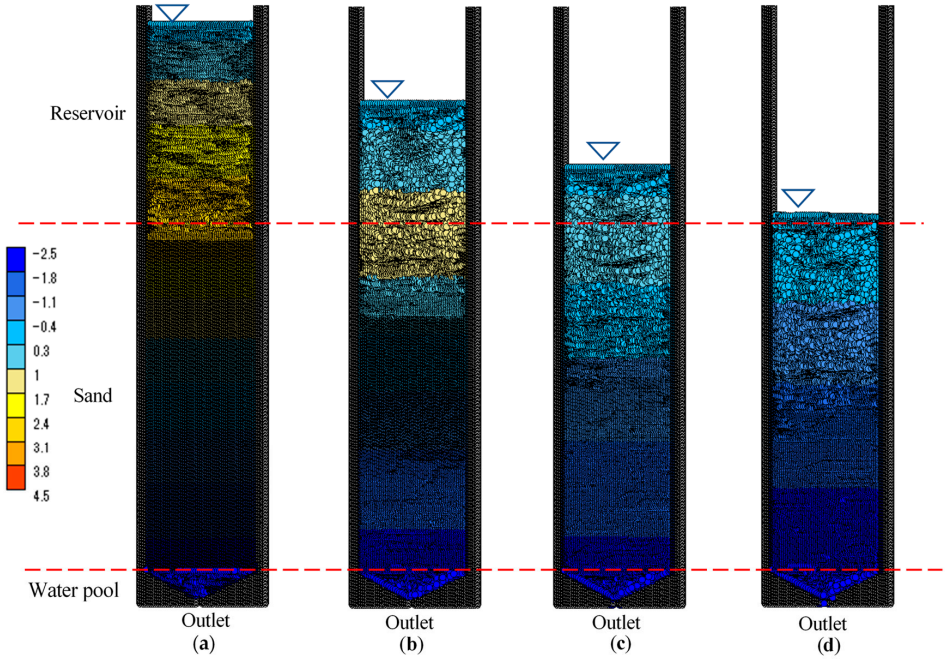


Figure 7. Comparison of the water pressure distribution in the results of the entire column apparatus numerical simulations when a reservoir was present. The horizontal scale is three times the vertical scale. Elapsed time at (**a**) 4 s, (**b**) 200 s, (**c**) 400 s, and (**d**) 600 s.

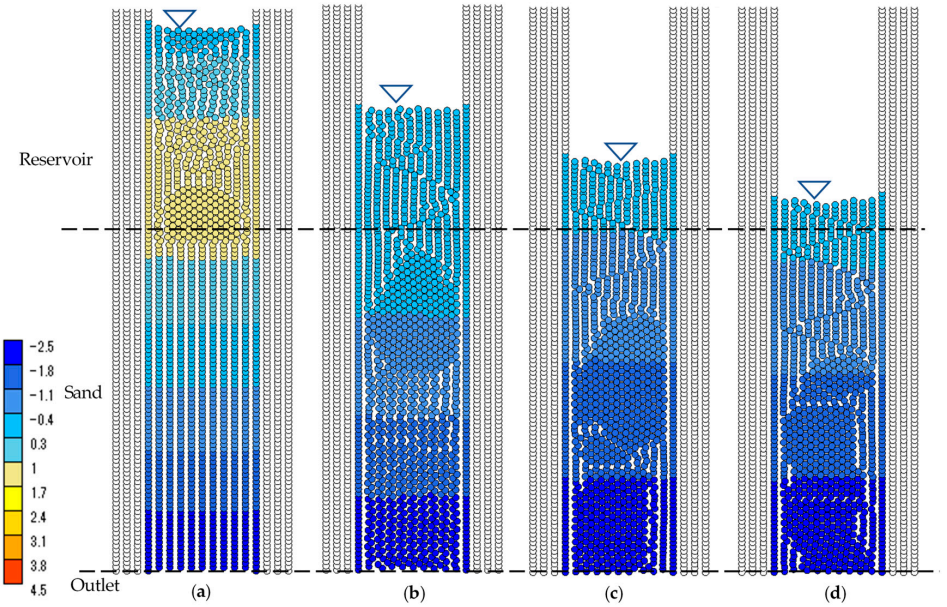


Figure 8. Comparison of the water pressure distribution in the results of the column-only numerical simulations when a reservoir was present. The horizontal scale is three times the vertical scale. Elapsed time at (**a**) 4 s, (**b**) 200 s, (**c**) 400 s, and (**d**) 600 s.

3.4. Comparison of the Results of the Numerical Simulations with the MPS Method and the Experimental Results

In Figure 9, the lowering of the free water surface in the reservoir is compared between the experimental and numerical simulation results. The experimental results are consistent with numerical simulation results obtained by the ASGMF method, a multi-flow method with coupled atmospheric gas, surface water, and groundwater [27]. By contrast, the free water surfaces obtained by the MPS method at an early elapsed time are lower than those obtained by the ASGMF simulation and the column experiment. The drawdown of the free water surface was 4.3 cm at the elapsed time of 20 s in the column-only simulation and 2.9 cm at the elapsed time of 32 s in the entire column apparatus simulation. In the column-only simulation, the water could easily flow out of the analytical domain without interruption because the open bottom edge of the numerical domain was the same diameter as the column. By contrast, in the entire column apparatus simulation, the plate with the water pool and the 4-mm-diameter outlet appended to the lower end of the analytical domain interrupted the outflow of water from the domain. The entire column apparatus simulation was conducted within a two-dimensional analysis domain with an area of 0.004 m × 1.0 m = 0.004 m^2, while the outlet of the column experiment was a circle with a diameter of 0.0034 m and an area of 9.1 × 10^{-6} m^2; thus, it was smaller than the area in the entire column apparatus simulation. This difference in the area of the outlet explains why the water level went down faster in the entire column apparatus simulation than in the column experiment. Thus, the drawdown of the free water surface was less in the column-only simulation than in the entire column apparatus simulation. The free water surface in the entire column apparatus simulation fell at the same rate as in the results of the column experiment and the ASGMF simulation, and at the elapsed time of 10 min, it was 1.3 cm lower than in the column experiment and the ASGMF simulation results. However, in the column-only simulation, the free water surface fell faster than in the experiment and the ASGMF simulation, and at the elapsed time of 10 min, it was 0.9 cm higher than in the experiment and the ASGMF simulation results. Therefore, the MPS method did not reproduce the drawdown of the free water surface in the reservoir as precisely as the ASGMF method, but the entire column apparatus simulation with the water pool and 4-mm-diameter outlet could approximately reproduce the drawdown of the free water surface in the reservoir. Furthermore, it was revealed in this study that the outlet and the overlying water pool affected the water flow in the column. The column-only simulations were conducted at several particle diameters that were equal to the initial space between two particles, and the final water pressure and particle distribution did not vary when the particle diameter was less than 0.005 m. Therefore, in the column-only simulations, the particle diameter of 0.005 m was the best with respect to both accuracy and computational cost. The computation time on a single core in the CPU (13th Gen Intel(R) Core (TM) i9-13900, Intel Corporation, Santa Clara, CA, USA) was about 24 h for a column-only simulation when the total number of particles was 2672. By contrast, in the entire column apparatus simulations, some water particles in the pool water did not exit via the 4 mm diameter outlet installed at the bottom of the column when the particle diameter was 0.002 m. As a result, in this case, the water level of the surface water in the column did not drop, and the height of the water level did not change until the end of the simulation. As described above, the water particles in the pool water were able to exit via the 4 mm diameter outlet when the particle diameter was 0.001 m. These results for the entire column apparatus simulations indicate that it is doubtful that a particle diameter of 1 mm, which is equal to the initial distance between two particles, is small enough for the 4-mm diameter outlet. Naturally, a particle diameter of 0.5 mm would be more physically suitable for reproducing the outflow via a 4-mm-diameter outlet. In the case of a 0.001 m

diameter, the computation time to reach an elapsed time of 80 min was about 480 h on 24 cores of the CPU described above.

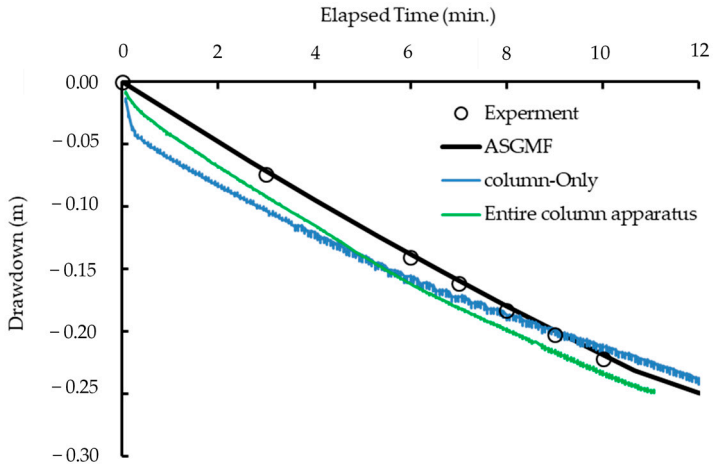


Figure 9. Comparison of the drawdown of the free water surface during drainage between the experimental results and the results of the column-only and the entire column apparatus numerical simulations using the MPS method and numerical simulations using the ASGMF method.

The arrangement of particles and the distribution of water pressure in the column-only and entire column apparatus simulations are shown in Figures 7 and 8. In both simulations, the arrangement of particles in the reservoir was already irregular at the elapsed time of 4 s, and the particles in the sand were also irregularly distributed by the elapsed time of 600 s. The free water surface in the reservoir was nearly flat, with no significant irregularities, in the column-only simulation; whereas, in the entire column apparatus simulation, the free water surface was completely flat regardless of the elapsed time. However, at the elapsed time of 200 s in the column-only simulation, the particles in the sand were gathered in one area, and this cluster of gathered particles subsequently grew. Furthermore, at the elapsed time of 600 s, a similar cluster of gathered particles appeared around the lower edge of the domain. These clusters migrated to the lower edge of the analytical domain. However, no such clustering was found in the distribution of particles in the entire column apparatus simulation. The water pressure gradually increased from zero at the free water surface to a maximum at the upper surface of the sand in both simulations (Figures 7 and 8). The water pressure in the sand decreased from the surface to −1.816 kPa, the value imposed at the lower boundary of the analytical domain. Moreover, the water pressure was not irregularly distributed in either the reservoir or the sand; in the entire column apparatus simulation, the water pressure distribution was also not irregular in the water pool and outlet. These tendencies are seen in Figure 10, which shows the vertical distribution of water pressure at the center of the analytical domain. The water pressure was almost 1 kPa higher in the entire column apparatus simulation than in the column-only simulation during the drawdown of the free water surface of the reservoir (Figure 10a–c). The reason for this water pressure difference between the simulations is that the water pool and the 4-mm-diameter outlet slowed the discharge of water from the column in the entire column apparatus simulation; whereas, in the column-only simulation, the water flowed out of the column smoothly and without resistance. However, when the free water surface approached the top of the sand surface, the water pressure in the entire column apparatus simulation was close to that in the column-only simulation (Figure 10d). In both simulations, there was no oscillation of the water pressure inside either the reservoir or the sand during the drawdown of the free water surface, and the water pressure decreased linearly to the lower edge of the analytical domain after linear increases from the free water surface to the surface of the

sand (Figure 10). Similarly, the water pressure in the water pool did not also oscillate but increased with depth. Therefore, this result clearly indicates the ability of MPS simulations to reproduce physical phenomena such as the resistance of fluid flow.

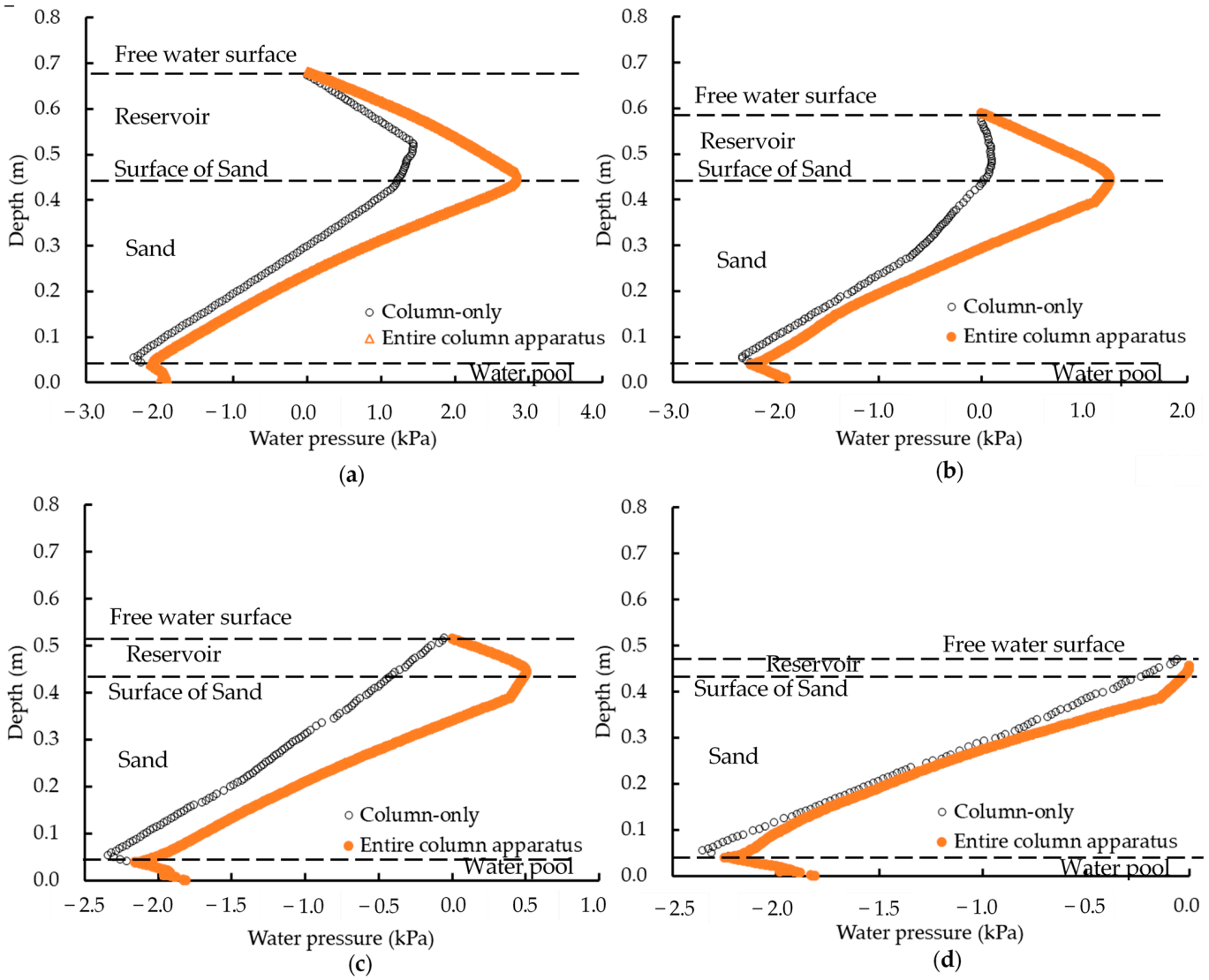


Figure 10. Comparison of the vertical distribution of water pressure when a reservoir was present in the results of the column-only and the entire column apparatus numerical simulations. Elapsed time at (**a**) 4 s, (**b**) 200 s, (**c**) 400 s, and (**d**) 600 s.

There was no water in the reservoir by the elapsed time of 776 s in the column-only simulation and by the elapsed time of 664 s in the entire column apparatus simulation. The arrangement of the particles after no water remained in the reservoir is shown in Figure 11. Water was still present in the reservoir at the elapsed time of 700 s in the column-only simulation (Figure 11a); whereas, in the entire column apparatus simulation, all water particles in the reservoir had infiltrated into the sand by the elapsed time of 700 s. In both simulations, the height of the top of the sand became constant after all water particles had infiltrated into the reservoir. However, the weight density of the particles in the column-only simulation was lower after the elapsed time of 776 s than before that time (Figure 11a–d). In particular, the distribution of particles in the upper part of the sand was much less dense at the elapsed time of 4800 s than at the elapsed time of 700 s (Figure 11a–d). With elapsed time, the mass of particles with a high weight density moved to the lower edge. By contrast, the distribution of particles in the entire column apparatus

simulation did not display a dense gathering of a mass of particles or an area with a lower weight density of particles (Figure 11e–h).

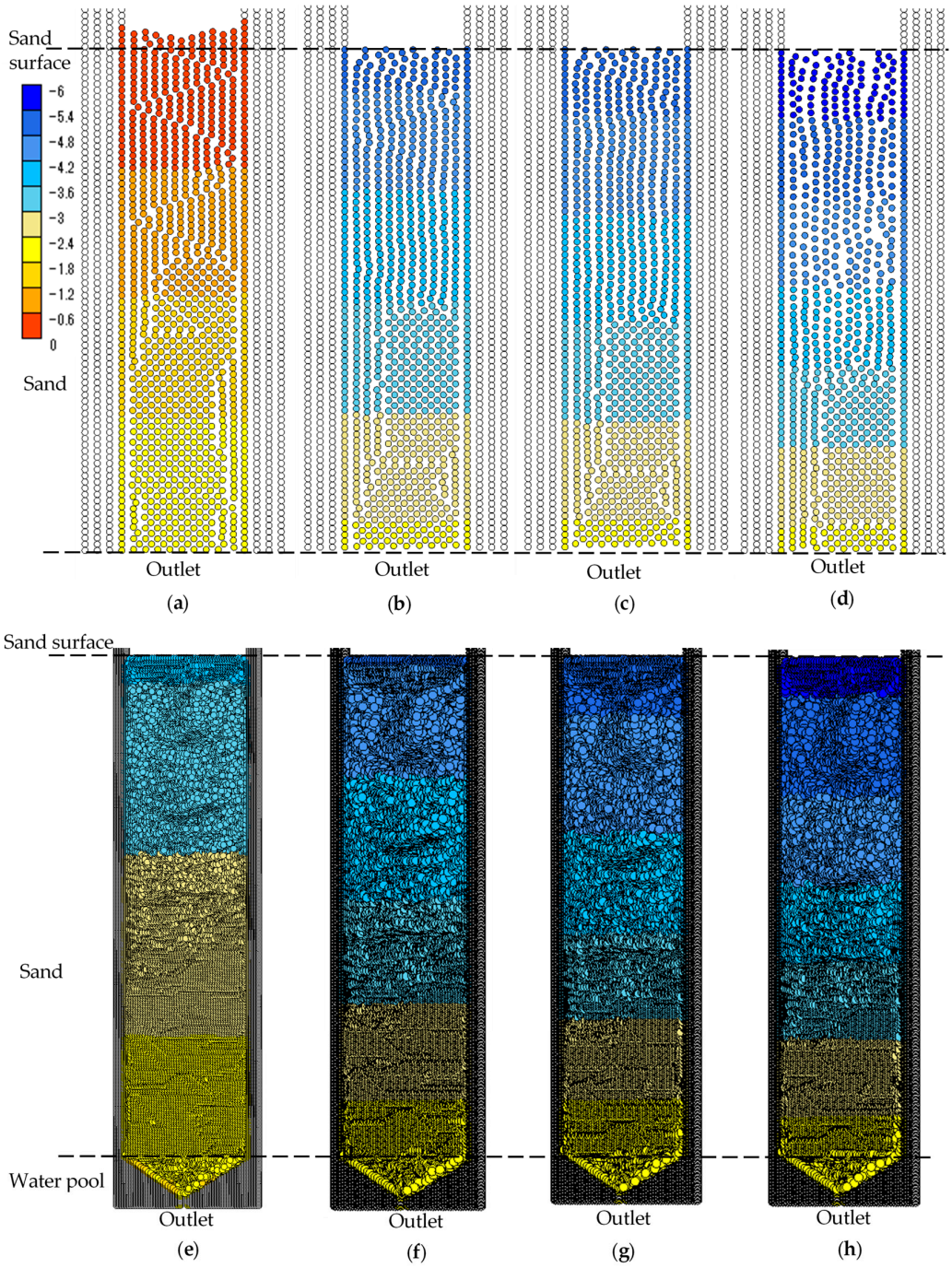


Figure 11. Comparison of the water pressure distribution when no reservoir was present in the results of the column-only and the entire column apparatus numerical simulations. The horizontal scale is twice the vertical scale. Elapsed time in the column-only numerical simulations at (**a**) 700 s, (**b**) 1200 s, (**c**) 1800 s, and (**d**) 4800 s. Elapsed time in the entire column apparatus numerical simulations at (**e**) 700 s, (**f**) 1200 s, (**g**) 1800 s, and (**h**) 4800 s.

Similar to the water pressure when there were still water particles in the reservoir, the water pressure decreased linearly to the imposed water pressure of −2.20804 kPa in the column-only simulation and to about −2.2 kPa in the entire column apparatus simulation at the lower boundary of the sand (Figure 12). When there were no water particles remaining in the reservoir, unlike when the reservoir contained water particles, the water pressure in

the sand in the entire column apparatus simulation was similar to that in the column-only simulation. Under this condition, the water pressure distribution did not oscillate in either simulation (Figure 12a–d). In addition, the water pressure at the top surface of the sand was not zero when there were no particles in the reservoir. This result indicates that the water pressure could be negative without being affected by the atmospheric pressure, and the water saturation could decrease to less than 1.0, at the boundary between the sand and the reservoir.

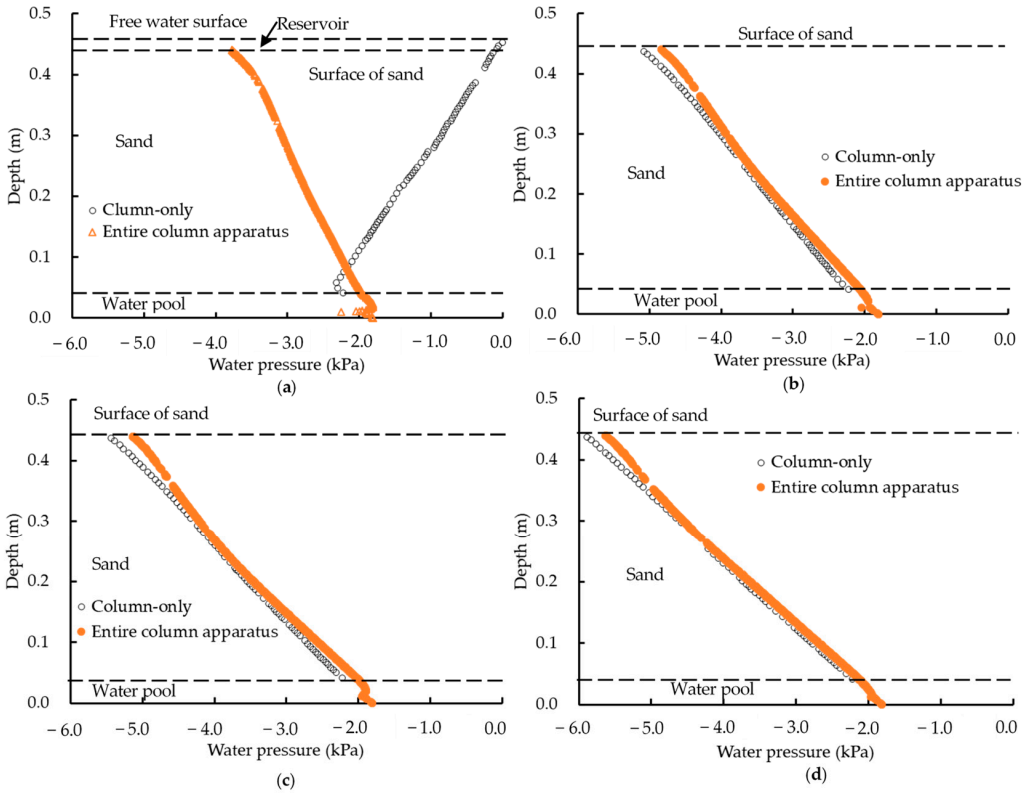


Figure 12. Comparison of the vertical distribution of the water pressure when no reservoir was present in the results of the column-only and the entire column apparatus numerical simulations. Elapsed time at (**a**) 700 s, (**b**) 1200 s, (**c**) 1800 s, and (**d**) 4800 s.

Figure 13 shows the variation of the water saturation in the sand with the elapsed time. The water saturation obtained by the ASGMF method precisely reproduced the experimental result, but the water saturation in the entire column apparatus simulation by the MPS method was almost 0.05 at the z coordinate of 39 cm and 0.08 at 24 cm, larger than the experimental results. On the other hand, at the z coordinate of 39 cm, the water saturation obtained by the MPS method in the column-only simulation was similar to that obtained by the ASGMF method and the column experiment. At the z coordinate of 24 cm, similar to the entire column apparatus simulation result, the water saturation in the column-only simulation by the MPS method was larger than that obtained experimentally and by the ASGMF method. Therefore, the MPS method was less accurate than the ASGMF method with respect to reproduction of the water saturation in the sand. However, the MPS method could reproduce the effect of the water pool and the 4-mm-diameter outlet because the water saturation in the entire column apparatus simulation was approximately 0.03 to 0.05 larger than that in the column-only simulation (Figure 13).

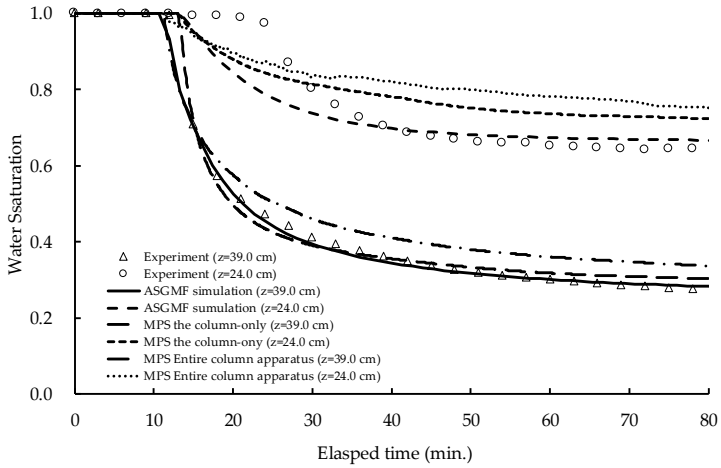


Figure 13. Comparison of the decrease in water saturation during drainage between the experimental and numerical simulation results obtained in the column-only and the entire column apparatus simulations by the MPS method and by the ASGMF method.

The water saturation values in the entire column apparatus simulation were slightly larger than those in the column-only simulation above the z coordinate of 0.2 m, except at the elapsed time of 700 s. On the other hand, the water saturation values in the entire column apparatus simulation were approximately consistent with those in the column-only simulation below z = 0.2 m (Figure 14). The water saturation in the column-only simulation at the elapsed time of 700 s was 1.0 throughout the sand region because some water particles remained in the reservoir (Figure 14a). In the entire column apparatus simulation, at the elapsed time of 700 s, no water particles remained in the reservoir, so the water saturation was already less than 1.0.

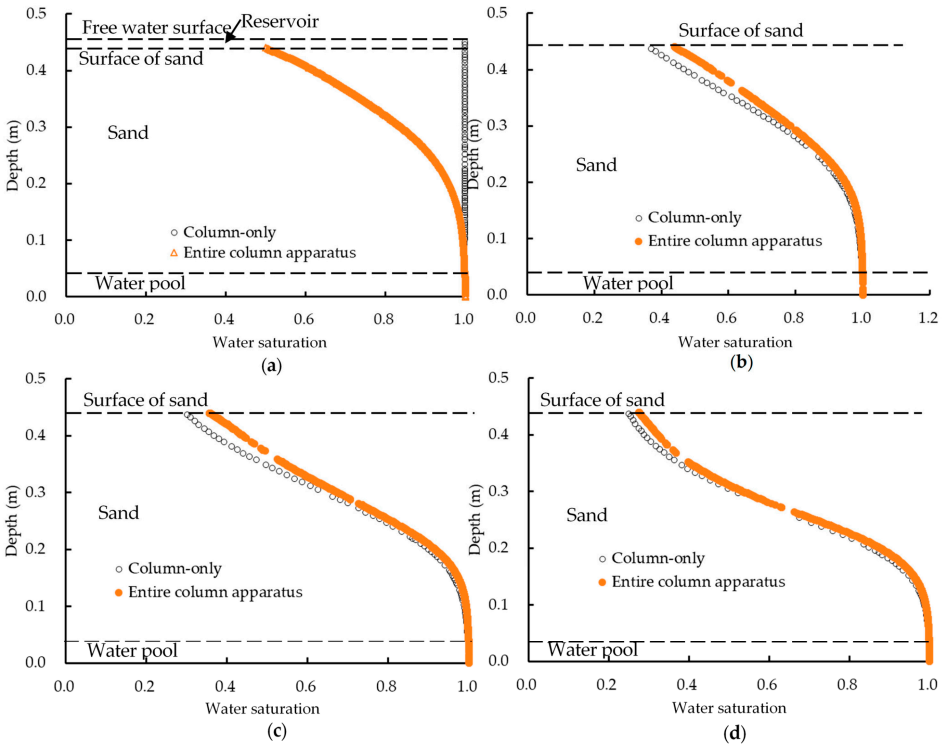


Figure 14. Comparison of the vertical distribution of water saturation when no reservoir was present in the results of the column-only and the entire column apparatus numerical simulations. Elapsed time at (**a**) 700 s, (**b**) 1200 s, (**c**) 1800 s, and (**d**) 4800 s.

As shown in Figure 12, the water pressure gradually decreased and became less than 1.0 at the upper boundary of the sand. Accordingly, as shown in Figure 14, the water saturation became less than 1.0 at the upper boundary of the sand and decreased along the curve of the van Genuchten model with the decrease of the water pressure, which was negative, similar to that in real, unsaturated sand.

4. Conclusions

In the developed numerical simulations, the water pressure of the SPPs can also be imposed as a non-zero gas pressure. Because the water pool and the outlet were filled with water particles, as presented in the results, the imposition of non-zero gas pressures of the SPPs made it possible to obtain a negative water pressure where the water had been extracted, which in this study was imposed as −3.0 kPa of the SPPs in the water pool. However, the standard SPP method, in which a water pressure of zero is imposed, can still be employed in the atmosphere, as shown by the distribution of particles and water pressure obtained in both the column-only and the entire column apparatus numerical simulations.

At an early elapsed time, the free water surface obtained with the MPS method went down more than in the experimental and the ASGMF method results: the free water surface was 4.3 cm lower at the elapsed time of 20 s in the column-only simulation and 2.9 cm lower at 32 s in the entire column apparatus simulation. As mentioned above, at an early elapsed time, the free water surface fell faster in the column-only simulation than in the column experiment, the numerical simulation by the ASGMF method, and the entire column apparatus numerical simulation by the MPS method. However, after the first large drawdown, the drawdown of the free water surface in the entire column apparatus simulation by the MPS method was always 1.3 cm lower, similar to that in the column experiment and the ASGMF method simulation. The water pressure was 1 kPa higher in the entire column apparatus simulation than in the column-only simulation. These results indicate that the water pool and the added outlet in the entire column apparatus simulation affected the water flow in the column.

The water pressure did not oscillate at any location or at any elapsed time in the developed numerical simulations, although the water pressure oscillates when the standard MPS method that uses the weight density of particles as the source term of the Laplacian equation for water pressure is applied. After no particles remained in the reservoir, the water pressure did not remain zero and eventually decreased to between −5.7 to 5.9 kPa, because there were no SPPs around the top surface of the sand at the boundary between the sand and the reservoir. As a result, the water saturation in the sand decreased from 1.0 along the curve of the van Genuchten model.

Therefore, the numerical simulations using the MPS method developed in this study could reproduce the drawdown in the column experiment, but the results were slightly less accurate, by about 1 cm, than those obtained with the ASGMF method. In addition, the developed numerical simulations could also reproduce the influence of an obstruction to the water flow and the negative water pressure of −2.2 kPa caused by water extraction. It is clear that this numerical simulation method can be applied to any porous medium with low permeability, such as sand, which here had an intrinsic permeability of 1.737×10^{-11} m^2, and that the MPS method can be used in many situations.

In another study, the author has developed an implicit deformation numerical simulation by using an elastic stress constitutive equation and the MPS method. It will be possible in the future to integrate this implicit deformation numerical simulation with the numerical simulation model developed in this study. Then, the numerical simulation method integrating the present numerical simulation method and the implicit deformation numerical simulation method will be used to evaluate the safety of dike failures when river water

overflows an embankment. At that time, it will be possible to employ a large-scale model to simulate a real embankment. For this purpose, the MPS method should be parallelized by using a GPU and CUDA or OpenACC and an MPI (Message Passing Interface).

Funding: This research received no external funding.

Data Availability Statement: Data are contained within the article.

Acknowledgments: I am grateful to Kei Nakagawa of Nagasaki University for giving me the opportunity to present this article. I am also grateful to my own institution, Meijo University, for providing annual research funding support.

Conflicts of Interest: The author declares no conflicts of interest. The funders had no role in the design of this study; in the collection, analyses, or interpretation of the data; in the writing of the manuscript; or in the decision to publish the results.

Abbreviations

The following abbreviations are used in this manuscript:

FDM	Finite Difference Method
FEM	Finite Element Method
GC	Gradient Correction
GPU	Graphics Processing Unit
HL	Higher Order Laplacian
HS	Higher Order Source Term
MPI	Message Passing Interface
MPS	Moving Particle Semi-Implicit Method
SPH	Smoothed-Particle Hydrodynamics Method
SPP	Space Potential Particle Method

References

1. Maeda, K.; Sakai, H.; Sakai, M. Development of seepage failure analysis method of ground smooth particle hydrodynamics. *Struct. Eng./Earth Eng.* **2006**, *23*, 307–319.
2. Harada, E.; Ikari, H.; Tazaki, T.; Gotoh, H. Numerical simulation for coastal morphodynamics using DEM-MPS method. *Appl. Ocean Res.* **2021**, *117*, 102905. [CrossRef]
3. LeVeque, R.J. *Finite Methods for Hyperbolic Problems*; Cambridge University Press: Cambridge, UK, 2002; pp. 64–86.
4. Hibi, Y.; Tomigashi, A. A numerical simulation model for a coupled porous medium and surface fluid system with multiphase flow. *J. Groundw. Hydrol.* **2018**, *60*, 409–434. [CrossRef]
5. Wen, X.; Zhao, W.; Wan, D. An improved moving particle semi-implicit method for interfacial flows. *Appl. Ocean Res.* **2021**, *117*, 102963. [CrossRef]
6. Ikari, H.; Yamono, T.; Goto, H. Multiphase particle method using an elastoplastic solid phase model for the diffusion of dumped sand from a split hopper. *Comput. Fluids* **2020**, *208*, 104639. [CrossRef]
7. Zhong, G.; Zha, R.; Won, D. MPS-FEM coupled method for 3D dam-break flows with elastic gate structures. *Eur. J. Mech. B/Fluid* **2022**, *94*, 171–189. [CrossRef]
8. Hibi, Y. Changes in the salt concentration distribution in surface water (seawater) due to seawater recirculation in a porous medium under tidal fluctuations. *J. Contam. Hydrol.* **2022**, *251*, 104090. [CrossRef]
9. Hibi, Y. Numerical model with moving particle method coupling groundwater. *J. Groundw. Hydrol.* **2024**, *66*, 3–17. [CrossRef]
10. Colagrossi, A.; Landrini, M. Numerical simulation of interfacial flows by smoothed particle hydrodynamics. *J. Comput. Phys.* **2003**, *191*, 448–475. [CrossRef]
11. Gotoh, H.; Ikari, H.; Memita, T.; Sakai, T. Lagrangian particle method for simulation of wave overtopping on a vertical seawall. *Coast. Eng. J.* **2005**, *47*, 157–181. [CrossRef]
12. Koshizuka, S.; Oka, Y. Moving-Particle Semi-Implicit Method for Fragmentation of Incompressible Fluid. *Nucl. Sci. Eng.* **1996**, *123*, 421–434. [CrossRef]
13. Khayyer, A.; Gotoh, H. Modified moving particle semi-implicit methods for the prediction of 2D wave impact pressure. *Coast. Eng.* **2009**, *56*, 419–440. [CrossRef]
14. Peyret, R.; Taylor, T.D. *Computation Methods for Fluid Flow*; Springer: New York, NY, USA, 2012; pp. 141–262.

15. Hill, A.A.; Straughan, B. Poiseuille flow in a fluid overlying a highly porous material. *Adv. Water Resour.* **2009**, *32*, 1609–1614. [CrossRef]
16. Onda, S.; Hosoda, T.; Jacimovic, N.; Kimura, I. Numerical simulation of dike erosion process due to overtopping flow. *J. Jpn. Soc. Civ. Eng.* **2014**, *2*, 168–175. [CrossRef]
17. Marion, M.; Teaman, R. Navier-stokes equations: Theory and approximation. *Handb. Numer. Anal.* **1998**, *6*, 503–689.
18. Matthew, W.F.; Fred, L.O. Numerical Solution of Richards' Equation: A Review of Advances and Challenges. *Soil Sci. Soc.* **2017**, *96*, 1257–1269.
19. Khayyer, A.; Gotoh, H. Enhancement of stability and accuracy of the moving particle semi-implicit method. *J. Comput. Phys.* **2011**, *230*, 3093–3118. [CrossRef]
20. Kondo, M.; Koshizuka, S. Improvement of stability in moving particle semi-implicit method. *Int. J. Numer. Methods Fluids* **2011**, *65*, 638–654. [CrossRef]
21. Khayyer, A.; Gotoh, H. A higher order Laplacian model for enhancement and stabilization of pressure calculation by MPS method. *Appl. Ocean Res.* **2010**, *32*, 124–131. [CrossRef]
22. Van Genuchten, M.T. A Closed-form equation for predicting the hydraulic conductivity of unsaturated soils. *Soil Sci. Soc. Am. J.* **1986**, *44*, 892–898. [CrossRef]
23. Mualem, P. A new model for predicting the hydraulic conductivity of unsaturated porous media. *Water Resurface Res.* **1976**, *12*, 513–522. [CrossRef]
24. Parker, J.C.; Lenhard, R.J. A model for hysteretic constitutive relations governing multiphase flow: 1. Saturation-pressure relations. *Water Resour. Res.* **1987**, *23*, 2187–2196. [CrossRef]
25. Tsuruta, N.; Khayyer, A.; Gotoh, H. A short note on dynamic stabilization of moving particle semi-implicit method. *Comput. Fluids* **2013**, *82*, 158–164. [CrossRef]
26. Tsuruta, N.; Khayyer, A.; Gotoh, H. Space potential particles to enhance the stability of project-based particle methods. *Int. J. Comput. Fluid Dyn.* **2015**, *29*, 100–119. [CrossRef]
27. Hibi, Y.; Tomigashi, A.; Hirose, M. Evaluation of a numerical simulation model for a system coupling atmospheric gas, surface water and unsaturated or saturated medium. *J. Contam. Hydrol.* **2015**, *183*, 121–134. [CrossRef]

Disclaimer/Publisher's Note: The statements, opinions and data contained in all publications are solely those of the individual author(s) and contributor(s) and not of MDPI and/or the editor(s). MDPI and/or the editor(s) disclaim responsibility for any injury to people or property resulting from any ideas, methods, instructions or products referred to in the content.